On the Structure and Stability of Three-Dimensional Laminar Separation Bubbles on a Swept Plate

Tilman Hetsch and Ulrich Rist

Institut für Aerodynamik und Gasdynamik, Universität Stuttgart,
Pfaffenwaldring 21, 70550 Stuttgart, Germany.
hetsch@iag.uni-stuttgart.de

Summary

A family of short leading-edge separation bubbles on a swept flat plate are investigated by means of direct numerical simulation (DNS) and spatial linear stability theory. An infinite swept plate with appropriate pressure distribution is a simple but suitable model for the mid-chord section of a swept wing or high lift device. A similar setup had therefore been chosen by Horton for his extensive experiments in this field in 1968. The main goal of the present study is to identify the influence of the sweep angle on the structure and stability of the flow through its systematic variation from 0° up to 60°. Due to the independence principle this influence on the base flow characteristics is only moderate. However, it does have a noticeable impact on stability. In contrast to the unswept two-dimensional (2D) case, *oblique* disturbance waves experience the highest amplification in swept cases.

1 Introduction

Due to strong adverse pressure gradients and low Reynolds numbers, separation bubbles are often encountered with high lift devices or on laminar airfoils of gliders. For instance, a transitional separation bubble was observed at the slat of an Airbus A310 [1]. Although the sweep angle of a modern passenger plane is of the order of 30°, so far numerical and experimental studies of separation bubbles have almost exclusively addressed the two-dimensional case.

The largest body of experimental data devoted to three-dimensional separation bubbles known to the authors was published by Horton in the late 1960s [2, 3]. Apart from Horton's benchmark data, literature on three-dimensional transitional separation bubbles is still rare. Davis and his coworkers successfully validated their boundary layer code with an inviscid-viscid interaction technique against Horton's data and thus confirmed his experiments [4]. More recently, Kaltenbach and Janke published a DNS of a transitional separation bubble in the flow behind a swept, rearward-facing step, with emphasis on its turbulent properties and sweep effects [5]. Up to an angle of 40° the mean flow followed the independence principle. The transition was reported to be triggered by a Kelvin-Helmholtz type instability of the shear-layer. Generally spatial growth rates increased with increasing sweep angle, though Kaltenbach and Janke found only a weak influence in their case.

Little is known about the transition mechanisms inside a 3D separation bubble, which are the key for understanding the global phenomena like control strategies or even the location of transition. There is the open question to which degree our knowledge of 2D separation bubbles is extensible to a 3D configuration. The present study represents a first step in this direction. We investigate the effect of sweep on the structure and stability of a steady, laminar separation bubble. The resulting "stream pipe" can serve as a *base flow* for disturbance calculations in the future.

2 Numerical Method and Case Description

For the calculation of leading-edge separation bubbles on an infinite swept plate a body fitted coordinate system is most suitable. The z- and x-direction are the parallel and normal to the leading-edge, respectively. All quantities in the paper are nondimensionalised by the reference length $\overline{L} = 0.05\,\mathrm{m}$ and the chordwise free-stream velocity $\overline{U}_\infty = 30\,\frac{\mathrm{m}}{\mathrm{s}}$, which was held constant for all cases. Different sweep angles Ψ were realized by varying the spanwise free-stream velocity $\overline{W}_\infty = \overline{U}_\infty \tan(\Psi)$. The calculations were performed with a global Reynolds number of $Re = \overline{U}_\infty \overline{L}/\nu = 100000$, although for physical interpretation the flow is better characterised by $Re_{\delta_1} = \overline{U}_\infty \delta_1(x_o)/\nu = 331$, based on the displacement thickness at the inflow. The rectangular integration domain is shown in Figure 2(a). As the leading-edge is itself not included in the calculation domain, a Falkner-Scan-Cooke (FSC) profile without pressure gradient is prescribed at the inflow boundary $x_o = 0.37$. The wall-normal coordinate y ranges from 0 to $y = 0.059 = 18 \cdot \delta_1(x_o)$.

The calculation of the base flow is based on the three-dimensional, incompressible Navier-Stokes equations in a velocity-vorticity formulation for an infinite swept plate:

$$\begin{aligned}
\frac{\partial\,\omega_x}{\partial\,t} + \frac{\partial\,(v\,\omega_x - u\,\omega_y)}{\partial y} &= \frac{1}{Re}\,\frac{\partial^2\,\omega_x}{\partial x^2} + \frac{\partial^2\,\omega_x}{\partial y^2}, & \frac{\partial^2\,u}{\partial x^2} &= -\frac{\partial^2\,v}{\partial x \partial y} \\
\frac{\partial\,\omega_y}{\partial\,t} - \frac{\partial\,(v\,\omega_x - u\,\omega_y)}{\partial x} &= \frac{1}{Re}\,\frac{\partial^2\,\omega_y}{\partial x^2} + \frac{\partial^2\,\omega_y}{\partial y^2}, & \frac{1}{Re}\frac{\partial^2\,v}{\partial x^2} + \frac{\partial^2\,v}{\partial y^2} &= -\frac{\partial\,\omega_z}{\partial x} \\
\frac{\partial\,\omega_z}{\partial\,t} + \frac{\partial\,(u\,\omega_z)}{\partial x} + \frac{\partial\,(v\,\omega_z)}{\partial y} &= \frac{1}{Re}\,\frac{\partial^2\,\omega_z}{\partial x^2} + \frac{\partial^2\,\omega_z}{\partial y^2}, & \frac{\partial^2\,w}{\partial x^2} &= -\frac{\partial\,\omega_y}{\partial x}\ .
\end{aligned}$$

The key assumption for an infinite swept wing is uniformity ($\frac{\partial}{\partial z} \equiv 0$) in spanwise direction for laminar calculations. This leads to a decoupling of the 2D-quantities u, v and ω_z, appearing in unswept calculations, from the new 3D-quantities ω_x, ω_y and w in the equation system above, which is known as the *independence principle*.

As a consequence, u, v, ω_z and any quantity derived directly from them do not depend on the sweep angle. The equations are discretised with fourth order central finite differences and integrated in a semi-implicit manner until steady state is reached. The steady calculation of the separation bubble is justified by its small size (e.g. the maximum backflow is $0.3\,\%\,\overline{U}_\infty$) and extensive computational experience from [6].

Note that due to the total absence of disturbances the base flow is purely laminar. The flow separates and re-attaches following the adverse pressure gradient which is implicitly introduced by the deceleration of the chordwise potential velocity $u_e(x)$ shown in Figure 3(c). There are two constant u_e plateaus at the beginning and at the end of the domain,respectively, which are connected smoothly by an analytical function. The whole setup represents the 3D extension of the two-dimensional leading-edge bubble investigated in [6], only with a slightly less u_e deceleration of $8.95\,\%\,\overline{U}_\infty$. More details concerning the general numerical method can be found in [7].

3 Flow Topology and Validation

The flow topology of the three-dimensional separation bubble shown in Figure 2(c) is exactly the same as the one sketched by Horton (Figure 2(b)). Just like in the experiments, the independence principle enforces leading-edge-parallel separation and re-attachment lines, here at the 2D-positions $x_S = 1.75$ and $x_R = 2.13$ for all sweep angles. The internal flow follows helical paths, resulting from the superposition of a w-component and the closed streamline loops known from 2D calculations. The symmetrical cross-section in the x-y plane of the separation bubble is simply a result of the laminar scenario. As demonstrated in [6] for the 2D case, the typical triangle-shaped outline develops under the presence of unsteady disturbances which trigger transition.

For the special case of vanishing z derivatives Moore has proven, that the general form of a "displacement surface" in 3D flows simplifies to the 2D definition of the displacement thickness $\delta_1(x)$ at any given z position [8]. Therefore it is correct to calculate δ_1, the momentum thickness δ_2 and the boundary layer thickness $\delta_{99.9}$ from u only, as in the unswept case. Figure 3(a) demonstrates that our code respects the independence principle, for the results are independent of Ψ. At the same time one can see that $\delta_{99.9}$ reaches only $80\,\%$ of the height of the integration domain, so it is well justified to assume potential flow at the upper boundary.

The step size independence of the numerical solution was investigated by grid refinement studies for the case $\Psi = 45°$. The standard resolution of 1394 and 97 grid points in x- and y-direction was independently halved and doubled. The maximum relative error with respect to the fine solution was then determined for all flow quantities $q \in \{u, v, w, \omega_x, \omega_y, \omega_z\}$ separately. The variation of the x-resolution yielded that the standard resolution was finer than necessary. The maximum deviation of the coarse solution to the fine one was $0.0017\,\%$, so 698 grid points would have been sufficient. The maximum error in y occurring in v is shown in Figure 3(b). Clearly, the coarse resolution of only 49 grid points in y is insufficient. But the maximum error of the standard resolution compared to the fine one is still $0.07\,\%$ and only visible in an enlarged cutout of Figure 3(b). It follows that the resolution of the calculation is good.

4 Base Flow: 3D Structure and Influence of Sweep

From the independence principle it is clear that u, v, ω_z, separation and reattachment positions as well as boundary layer thickness are identical to the 2D case for any sweep angle. This 2D flow is merely *superimposed* with a w-velocity component which grows in strength with increasing sweep angle. The separation bubble has only an indirect influence on w through the displacement thickness shown in Figure 3(a). This is indicated by the w-isolines displayed in Figure 3(c) which show no special behaviour inside the bubble, but generally follow the trend of δ_1. The w profiles increase linearly from the wall, and in close-ups near the wall no influence of the bubble is visible. This was to be expected from the continuity equation which simplifies to its 2D form because $\partial / \partial z \equiv 0$. For the same reason the general definitions of ω_x and ω_y simplify to $\omega_x = -\frac{\partial w}{\partial y},\ \omega_y = \frac{\partial w}{\partial x}$, so that these quantities are bound to show the same behaviour as w. Note that the w profiles exhibit an inflexion point which is more easy to spot in the crossflow profiles w_s. As an overview, Figure 1 shows the downstream development of the streamline-oriented velocity components u_s and w_s for $\Psi = 30^\circ$: due to constant u_e at the upper boundary there is no crossflow present at the inflow. Within the bubble, a strong w_s-component is induced by the local u_e deceleration. Finally, near the outflow the flow is asymptotically approaching FSC-characteristics, but a weak crossflow is still existent.

The effect of sweep on the base flow can exemplarily be seen in the crossflow profile w_s at the separation line in Figure 3(d). Increasing sweep increases the absolute value of a 3D quantity without changing its form. From looking at the locally normalised version of the same profiles, shown in Figure 3(e), it is obvious that the sweep angle simply scales a sweep-independent prototype profile. This is also true for w profiles at any position, as demonstrated in Figure 3(e) far downstream, and therefore also holds for ω_x and ω_y. Because of $w_e \equiv \overline{W}_\infty / \overline{U}_\infty$ the nondimensionalised profiles of w, ω_x, ω_y scale with the global factor $\tan(\Psi)$ like their values at the upper boundary. After normalisation all swept profiles coincide with the one at $\Psi = 45^\circ$, which can be seen as the generic solution. The streamline-oriented w_s-profiles on the other hand can only be normalised *locally* for their indirect dependency on $u_e(x)$:

$$w_s(x,y) := -u(x,y) * \sin(\varphi_{\mathrm{pot}}) + w(x,y) * \cos(\varphi_{\mathrm{pot}}),$$

with $\varphi_{\mathrm{pot}} = \arctan(W_\infty / u_e(x))$.

5 The Influence of Sweep on the Flow Stability

Despite the only moderate influence of sweep on the laminar flow it has a noticeable influence on its stability. The inflection point in the swept crossflow profiles gives rise to a inviscid instability which is not present in the unswept case. For example, steady crossflow vortices with a frequency of $0\,\mathrm{Hz}$ become weakly amplified. Figure 6 summarises the results from three-dimensional spatial linear stability theory. Figure 4(e) gives an overview over the whole integration domain. The separation

and re-attachment locations are marked with *S* and *R*, respectively. The graph shows the spatial amplification rate $-\alpha_i$ as a function of x and the frequency β of the disturbance. It is valid for all sweep angles as a vanishing spanwise wavenumber $\gamma = 0$ cancels the influence of w in the Orr-Sommerfeld and the Squire equation. At the separation point $x_s = 1.75$ the spatial amplification is displayed in cross sections for $\Psi = 0^\circ, 15^\circ, 30^\circ$ and 45° in Figures 4(a) through 4(d). The initially symmetrical distribution in the planar case is more and more distorted and the amplification maximum moves to oblique waves with positive γ. In accordance with the findings in [5] increasing growth rates are observed for increasing sweep angles. In Figure 4(f) the position of the amplification maxima are marked relative to the 2D maximum. All relevant data of these maxima are summarised in table 1. According to the evaluated sweep angles the propagation direction of the most amplified wave seems to be in the order of 10° less than the considered sweep angle. A comparison yields that the maximum amplification in the $\Psi = 45^\circ$ case is $7\,\%$ higher than in the 2D case.

6 Conclusions

A family of three-dimensional laminar separation bubbles on an infinite swept plate has been successfully calculated and validated. An investigation of the effect of sweep on the flow yielded the following results:

- Due to the independence principle the separation bubble is only moderately influenced by the sweep angle: The 3D quantities w, ω_x and ω_y are superimposed on the 2D quantities u, v and ω_z without changing the general flow topology. The sweep angle merely scales the "generic" solution $\Psi = 45^\circ$ in w, ω_x and ω_y with a global factor of $tan(\Psi)$. These features make the calculated flow an ideal candidate for disturbance investigations: All properties of the flow are now known. As no new features of the flow appear for higher sweep angles, the effects of sweep are isolated and the sweep angle is the only possible cause of any interesting phenomenon to be observed.
- Despite of the simple structure and although two-dimensional disturbances are amplified *earlier* according to Squire's theorem, the amplification rates of oblique waves are up to $7\,\%$ *stronger* in the case $\Psi = 45^\circ$. For 3D flows it is therefore generally not sufficient to restrict oneself to the investigation of 2D waves when determining basic properties like N-factors.

Acknowledgements

The authors would like to thank Professor Gaster and Dr. Horton from the Queen Mary College, University of London, for providing us with a copy of Horton's thesis and allowing us to reprint a figure from it. The financial support by the Deutsche Forschungsgemeinschaft (DFG) under contract number Ri 680/12-1 is gratefully acknowledged.

References

[1] E. Greff: “In-flight Measurements of Static Pressures and Boundary-Layer State with Integrated Sensors”, J. Aircraft, *28*, No. 5, (1991), pp. 289-299.

[2] H. Horton: “Some Results of Investigations of Separation Bubbles”. AGARD **CP-4**, (1966), pp. 779–811.

[3] H. Horton: “Laminar Separation Bubbles in Two and Three Dimensional Incompressible Flow”. PhD thesis, Department of Aeronautical Engineering, Queen Mary College, University of London, (1968).

[4] R. Davis, J. Carter, E. Reshotko: “Analysis of Transitional Separation Bubbles on Infinite Swept Wings”. AIAA Vol. **25**, No. 3, (1987), pp. 421–428.

[5] H. Kaltenbach, G. Janke: “Direct numerical simulation of flow separation behind a swept, rearward-facing step at $Re_{\mathrm{H}} = 3000$”. Phys. Fluids, **12**, (2000), pp. 1220–2337.

[6] U. Rist: “Zur Instabilität und Transition laminarer Ablöseblasen”. Habilitation, Universität Stuttgart, Shaker Verlag, (1999).

[7] P. Wassermann: “Mechanisms and passive control of crossflow-vortex-induced transition in a three-dimensional boundary layer”. J. Fluid Mech., **456**, (2002), pp. 49–84.

[8] F. Moore: “Displacement Effect of a Three-Dimensional Boundary Layer”. NACA Report 1124, (1953).

Table 1 Parameters of the most amplified disturbance for various sweep angles Ψ: spatial amplification rate $-\alpha_i$, chordwise wavenumber α_r, spanwise wavenumber γ, frequency β, the local propagation direction $\varphi = \arctan(\gamma/\alpha_r)$ and the difference $\Delta\varphi = \Psi - \varphi$.

Ψ	$-\alpha_{i_{\mathrm{Max}}}$	α_r	γ	β	φ	$\Delta\varphi$
0°	10.89	47.32	0.00	17.17	0.0°	0.0°
15°	10.95	46.54	5.76	17.53	7.0°	-8.0°
30°	11.17	42.73	14.43	18.99	18.6°	-11.5°
45°	11.65	36.20	25.01	23.90	34.6°	-10.4°

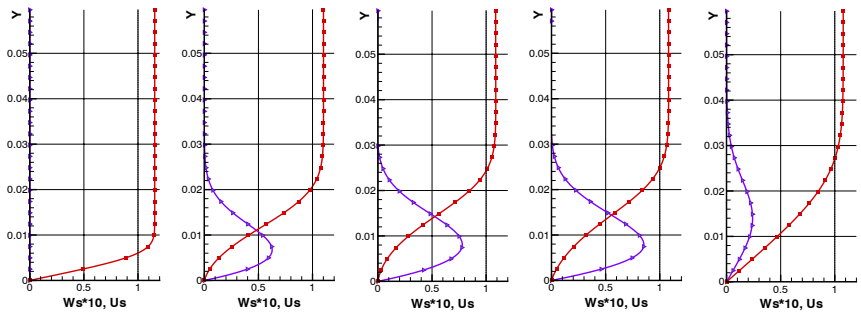

Figure 1 Streamline-oriented velocity profiles u_s (square), w_s (triangle) at the inflow, at separation, at the middle of the bubble, at reattachment, far downstream at $x = 4.4$.

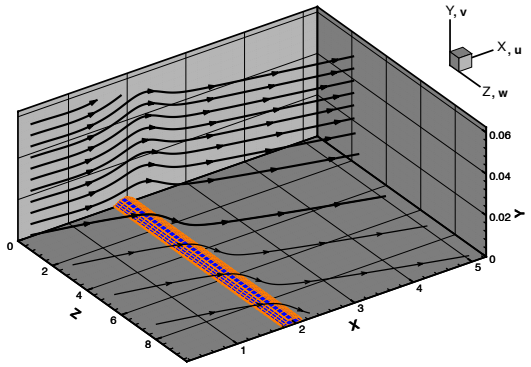

(a) $\Psi = 30^\circ$: the entire integration domain.

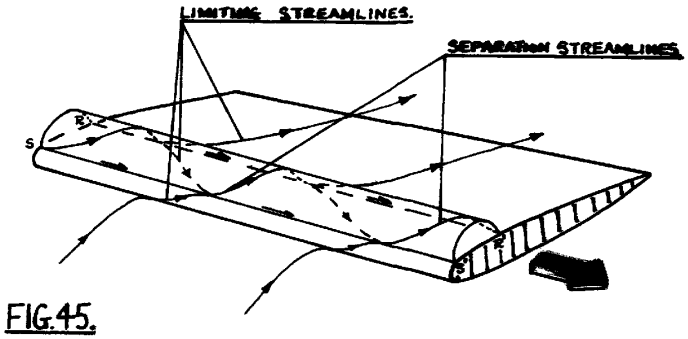

(b) Horton's model of a leading-edge bubble taken from [3].

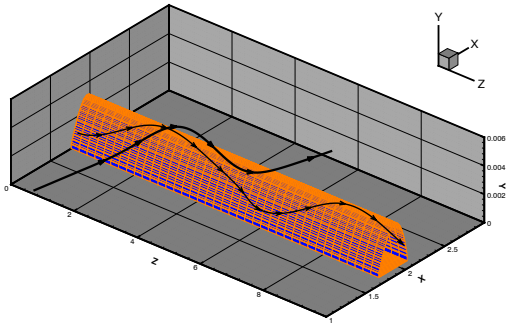

(c) Internal & external streamlines in simulation.

Figure 2 Global flow topology of a separation bubble on a infinite swept plate.

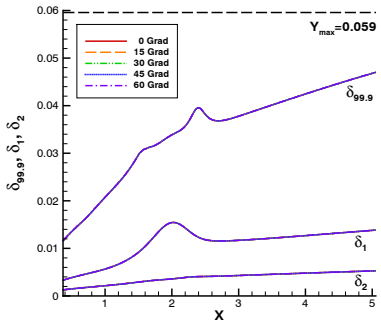

(a) The sweep independent boundary layer thicknesses.

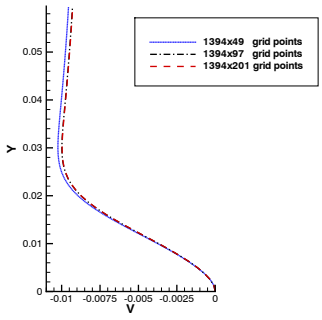

(b) Step size test with 49, 97 and 201 grid points in y .

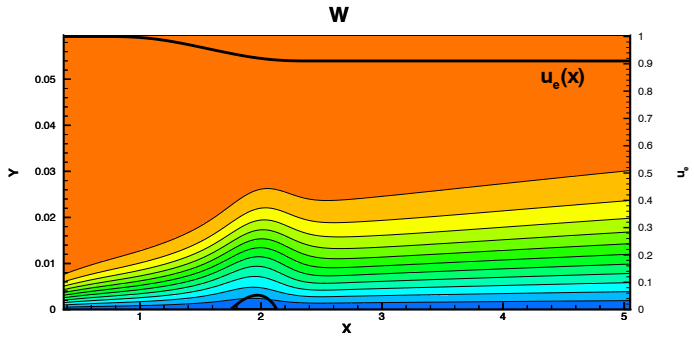

(c) Overview over the w-component and u at the upper boundary.

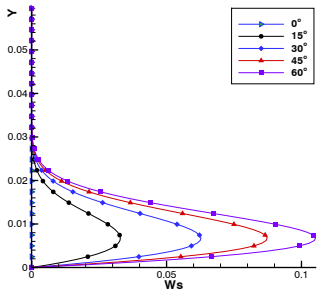

(d) Crossflow profiles at $x_s = 1.75$ for different sweep angles.

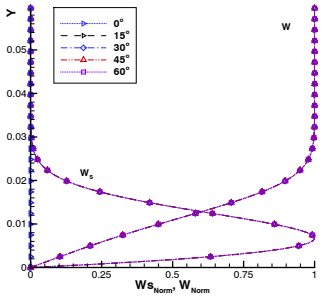

(e) w_s at $x = 1.75$, w at $x = 4.4$ both normalised.

Figure 3 Laminar flow properties and influence of sweep

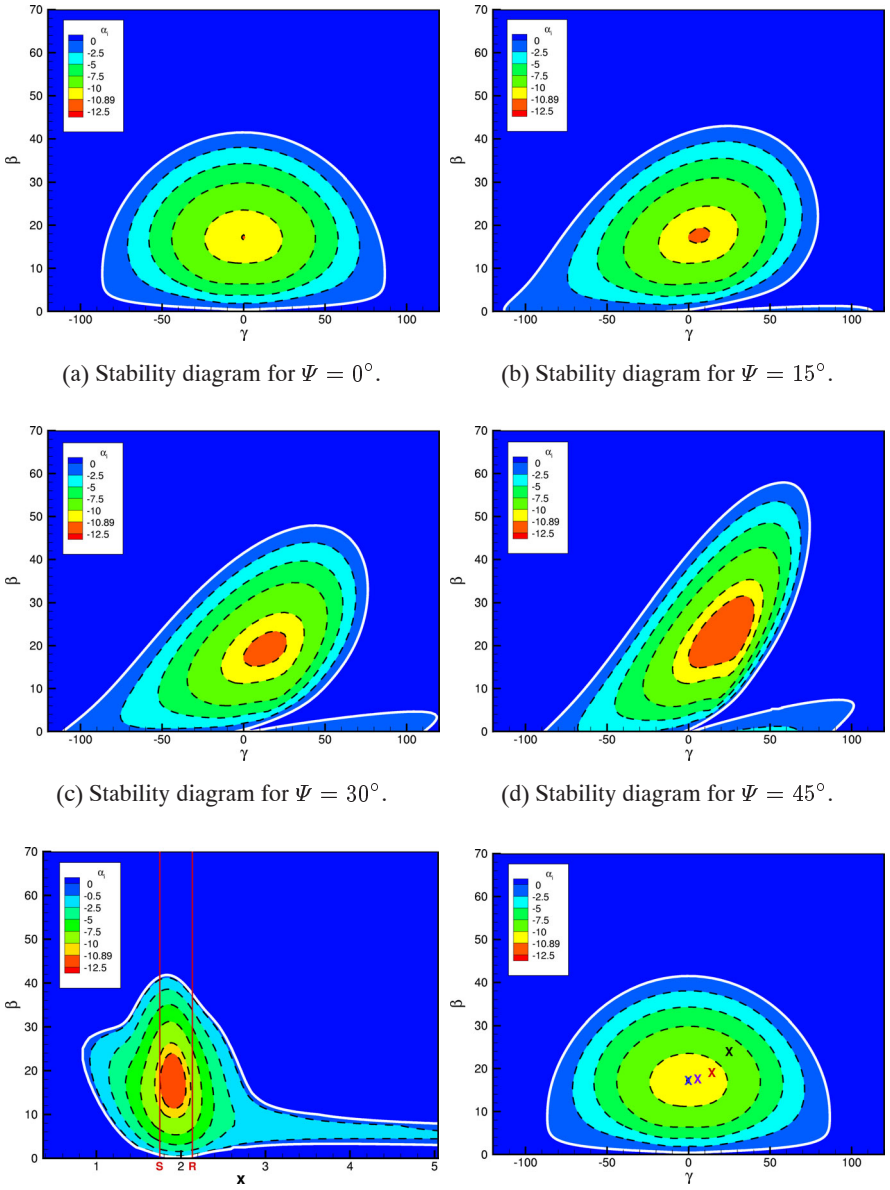

(a) Stability diagram for $\Psi = 0^\circ$.

(b) Stability diagram for $\Psi = 15^\circ$.

(c) Stability diagram for $\Psi = 30^\circ$.

(d) Stability diagram for $\Psi = 45^\circ$.

(e) Stability diagram $\alpha_i(x, \beta)$ with fixed $\gamma = 0$ (for all Ψ).

(f) Position of α_i-Minimum for all Ψ's: plotted into the $\Psi = 0^\circ$ case.

Figure 4 Linear stability theory results at $x = 1.75$ (separation line) versus frequency β and spanwise wavenumber γ. The white curve corresponds to neutral stability. The innermost contour level is kept constant at the minimal spatial growth rate $\alpha_i = -10.89$ of the case with sweep angle $\Psi = 0^\circ$.